Heliyon 7 (2021) e06043

Contents lists available at ScienceDirect

Heliyon

journal homepage: www.cell.com/heliyon

Research article

Multi-objective cutting parameter optimization model of multi-pass turning in CNC machines for sustainable manufacturing

Phengky Pangestu, Eko Pujiyanto, Cucuk Nur Rosyidi *

Department of Industrial Engineering, Universitas Sebelas Maret, Surakarta 57126, Indonesia

ARTICLE INFO

Keywords:
Cutting parameters optimization
Multi-objective
Multi-pass turning
Sustainable manufacturing

ABSTRACT

Sustainable manufacturing has grown widely owing to recent environmental issues. This study aims to develop a multi-objective multi-pass turning optimization model to determine the optimal cutting parameters, including spindle rotation speed, feed rate, depth of cut, and number of roughing passes. The optimization model considers several criteria in the key metrics of sustainable manufacturing, i.e., energy consumption, carbon emissions, production time, and production cost. A numerical example is provided to show the application of the model, including sensitivity analysis, to study the effects of several cutting parameters on the objective functions. The model can be used by manufacturing industries to improve their manufacturing process efficiency and simultaneously produce products that support sustainable manufacturing.

1. Introduction

Global warming is one of the major environmental issues due to high carbon emissions. According to the International Energy Agency (2007), manufacturing processes contribute to approximately 36% of carbon dioxide emissions by consuming almost one-third of the global energy consumption. This has led to the emergence of various policies, such as carbon emission taxes, as a form of commitment to the Kyoto Protocol to reduce carbon dioxide emissions and five other greenhouse gases. The challenges are quite difficult for the manufacturing industries to bear the economic burden. Therefore, the manufacturing sector needs to arrange low-carbon manufacturing without increasing costs and reducing production efficiency.

The need for sustainable products and processes initiates the concept of sustainable manufacturing to create products with economic value through a process by minimizing negative impacts on the environment, saving the use of energy and natural resources, and preserving them to guarantee future availability (Amaranti et al., 2017). There are six key metrics for sustainable manufacturing (Jawahir and Dillon, 2007). Three of these are easily quantified, i.e., energy consumption, manufacturing cost, and waste management, while the other three are not easily quantified, i.e., operational safety, personal health, and environmental impact. According to Eaton (1999), these metrics must meet the needs of all stakeholders, facilitate innovation and growth, align business units from different geographical locations, be compatible with related measurement needs, and measure the appropriate components.

A manufacturing process is a procedure designed to produce physical or chemical changes to a material to add value to it (Groover, 2012). The manufacturing industry uses many types of machines to support manufacturing processes. One of the most important machines in the manufacturing process is computer numerical control (CNC) turning. There are two types of CNC turning operations: single-pass turning and multi-pass turning. Single-pass turning assumes a constant depth of cut (Hu et al., 2019). Multi-pass turning may consist of roughing, semi-finishing, and finishing passes with different depths of cut. In multi-pass turning, the total cutting depth is determined by the number of passes until it reaches the final diameter. This causes multi-pass turning optimization to be more complex than single-pass turning, and is more relevant for application in the manufacturing industry (Vipin et al., 2011).

One of the advantages of CNC turning machines is their higher accuracy compared to that of conventional machines. Nevertheless, the use of CNC turning machines is costly. In addition, the negative impact on the environment caused by the energy consumption of CNC machines (turning and milling) in the manufacturing process is approximately 99% (Zhong et al., 2017). The impact can be reduced by applying several metrics for sustainable manufacturing. The application of these metrics can be achieved by formulating a mathematical model to find the optimal cutting parameters through multi-objective optimization, allowing for a

* Corresponding author.
E-mail address: cucuknur@staff.uns.ac.id (C.N. Rosyidi).

https://doi.org/10.1016/j.heliyon.2021.e06043
Received 19 July 2020; Received in revised form 19 September 2020; Accepted 18 January 2021

trade-off between several conflicting issues (Gunantara, 2018). Multi-objective optimization has been employed in diverse research fields such as product design, operations management, and manufacturing processes. For more details about multi-objective optimization, please refer to Marler and Arora (2005).

Many studies have developed a cutting parameter optimization model of CNC turning that considers sustainable manufacturing and machining efficiency both analytically and experimentally/empirically. Chen and Tsai (1996) developed an optimization model and solved it using an algorithm based on simulated annealing and Hooke-Jeeves pattern search to minimize production costs in a multi-pass turning operation. Mativenga and Rajemi (2011) determined the optimal cutting parameters to achieve minimum energy consumption, which includes energy during setup operation, energy during cutting, energy for tool replacement, and energy embodied in the tool and workpiece. Li et al. (2013) presented an analytical model to calculate carbon emissions generated from several sources in a CNC-based machining system, namely electricity consumption, tool, cutting fluid, raw material, and fabrication of chip removal. Chauhan et al. (2015) developed an optimization model to minimize the production cost in multi-pass turning by using chaotic particle swarm optimization. Yi et al. (2015) identified the correlation between cutting parameters and carbon emissions in the model of Li et al. (2013), as well as the cutting parameters to achieve the minimum production time. Lu et al. (2016) investigated an energy-efficient multi-pass turning operation and proposed a multi-objective backtracking search algorithm to solve the model. Liu et al. (2016) developed a numerical model to optimize cutting parameters to minimize the carbon emission cost considering carbon tax policies as well as production time. Zhou et al. (2017) developed a model to determine carbon emissions in a machining process generated from raw materials, energy consumption, and waste. Widhiarso and Rosyidi (2018) developed a multi-objective optimization model to minimize production costs and environmental impact. Tian et al. (2019) developed a multi-objective cutting parameter optimization by considering the tool wear conditions. Bagaber and Yusoff (2019) integrated the energy and cost for multi-objective optimization in a sustainable turning process. Their research considered the dry and wet cutting processes. Hu et al. (2019) developed cutting parameter optimization in single-pass turning to minimize energy consumption by considering cutting and non-cutting operations. Table 1 summarizes the related literature and the position of this research, especially the analytical optimization model.

According to the above studies, there is a gap in research, especially in the analytical model of integrated machining energy consumption. Generally, energy consumption is calculated based on the black-box and bottom-up approaches (Guo et al., 2015). The black-box approach model has a clearer form of total energy consumption during machining compared to the bottom-up approach. In the black-box approach, energy consumption is established by a function that relates the cutting parameters and the corresponding energy using specific coefficients. Hu et al. (2019) developed an integrated model considering both the cutting and non-cutting energy consumptions based on the black-box approach. This is because non-cutting energy consumption has not been explored in previous research, especially the changes in spindle rotation. Non-cutting energy consumption can exceed 30% of the total energy consumption. However, this model is only suitable for single-pass turning operations. Moreover, some important constraints in the machining process, such as the chip-tool interface temperature, tool life, and stable cutting region, are not considered. In addition, no research has been conducted to find the optimal cutting parameters to minimize energy consumption, carbon emissions, production cost, and production time simultaneously.

Therefore, this research aims to develop a multi-objective cutting parameter optimization model for the multi-pass turning process. The contribution of the model is in the inclusion of non-cutting energy consumption in multi-pass turning and that it considers several decision variables, i.e., spindle rotation speed, feed rate, and depth of cut, to minimize energy consumption, carbon emission, production cost, and

Table 1. Analytical machining optimization models.

Authors (year)	Machining process	Cutting parameters					Objective functions				
		Cutting speed	Spindle rotation speed	Feed rate	Depth of cut	Number of roughing pass	Tool wear	Carbon emission	Energy consumption	Production cost	Production time	Machining precision
Chen and Tsai (1996)	Multi-pass turning	✓	×	✓	✓	✓	×	×	×	✓	×	×
Mativenga and Rajemi (2011)	Multi-pass turning	✓	×	✓	✓	✓	×	×	✓	×	×	×
Li et al. (2013)	Single-pass turning	✓	×	✓	×	×	×	✓	×	×	×	×
Chauhan et al. (2015)	Multi-pass turning	✓	×	✓	✓	✓	×	×	×	✓	×	×
Yi et al. (2015)	Single-pass turning	✓	×	✓	×	×	×	✓	×	×	✓	×
Lu et al. (2016)	Multi-pass turning	✓	×	✓	✓	✓	×	×	✓	×	×	✓
Liu et al. (2016)	Single-pass turning	✓	×	✓	×	×	×	✓	×	×	✓	×
Zhou et al. (2017)	Turning, milling & drilling	✓	×	✓	×	×	×	✓	×	×	×	×
Widhiarsio and Rosyidi (2018)	Single-pass turning	✓	×	✓	×	×	×	✓	×	✓	×	×
Tian et al. (2019)	Turning, milling & drilling	✓	×	✓	×	×	✓	✓	×	✓	✓	×
Bagaber and Yusoff (2019)	Single-pass turning	✓	×	✓	×	×	×	×	✓	✓	×	×
Hu et al. (2019)	Single-pass turning	×	✓	✓	×	×	×	×	✓	×	×	×
This research	Multi-pass turning	×	✓	✓	✓	✓	×	✓	✓	✓	✓	×

production time. The model in this research may be considered as the extension model of Hu et al. (2019) from single-pass turning to multi-pass turning, which is more often found in the manufacturing industry for economic reasons (Chen and Tsai, 1996). In addition, this research is also based on Lu et al. (2016) in formulating multi-pass turning operations, Tian et al. (2019) in formulating production cost, and Yi et al. (2015) in formulating carbon emissions. The normalization approach is used in this research to solve multi-objective optimization, as suggested by Marler and Arora (2005), owing to its robustness.

The remainder of this paper is organized as follows. Section 2 presents the problem definition of the CNC turning system. Section 3 presents the model development of the multi-objective cutting parameters of the multi-pass turning process. A numerical example is given in Section 4 to show the applicability of the model. Finally, the conclusions and future work are presented in the last section.

2. Problem definition

In this research, a multi-pass turning operation consists of a roughing pass and a finishing pass. It was modeled by considering several aspects: (1) sustainable manufacturing in terms of energy consumption, carbon emissions, and production cost, and (2) machining efficiency in terms of production time. CNC turning systems often involve one or more CNC machines during production (Li et al., 2013). The inputs of this system are electrical energy and raw materials. During the machining process, each machine is equipped with tools and fixtures to produce output in the form of finished products and removed material (chip). A typical CNC turning system is shown in Figure 1.

Reducing carbon emissions and production costs are two supporting components of sustainable manufacturing. Based on Figure 1, carbon emissions and production costs are generated from tools, raw materials, energy consumption (electricity), and chips indirectly. However, cutting parameters during the machining process have little impact on raw materials and chips (Yi et al., 2015). Thus, raw materials and chips were not considered in our carbon emission and production cost models. Moreover, production costs consist of management and manpower, which are calculated based on production time, which depends on the cutting parameters.

CNC turning machines are inseparable from the need for energy consumption during the machining process (Hu et al., 2019). Energy consumption comprises cutting and non-cutting energy consumptions. Cutting energy consumption deals with the direct use of energy to cut a workpiece, while non-cutting energy consumption deals with the energy consumed during the non-cutting process consisting of the tool path and spindle rotation speed change. The tool path energy consumption is the energy consumed to move the tool to the right position before cutting begins. The energy consumption of changes in the spindle rotation speed is the energy used for spindle acceleration or deceleration. The energy consumption of CNC turning (Hu et al., 2019) is shown in Figure 2.

The determination of the cutting parameters in the multi-pass turning operation can affect the cutting and non-cutting energy consumption, which will cause a conflict between the two. An illustration is shown in Figure 3, where workpiece Y is machined by a CNC turning machine. There are two cutting parameters schemes for processing a workpiece Y, i.e., (a) 720 rpm and 0.30 mm/rev for the roughing pass as well as 1,080 rpm and 0.30 mm/rev for the finishing pass; (b) 1,080 rpm and 0.30 mm/rev for the roughing pass as well as 1,440 rpm and 0.30 mm/rev for the finishing pass. In this process, the red lines indicate the tool path with one or more roughing passes and a one-time finishing pass. Then, the notations of "↺" and "↻" indicate spindle acceleration and deceleration, respectively, as shown in Figure 3.

Based on Figure 3, non-cutting activities are depicted by Y_1, Y_2, Y_3, Y_4, and Y_5. In processing Y_1 and Y_5, the rapid and spindle rotation speed was set to 0 rpm to reduce energy consumption. Therefore, these activities were excluded. The process of Y_4 is closely related to the transmission line, lubrication, and spindle rotation speed (Lu et al., 2016). Assuming that there is no change in the transmission line and lubrication condition, only the acceleration and deceleration of the spindle will affect the process of Y_4.

Figure 4 illustrates the power profiles of the cutting parameter schemes, as previously explained. There are four different areas: (1) the forward slashes represent the energy consumption of the spindle acceleration, (2) the blue grids represent the energy consumption of the tool path, (3) the red grids represent the cutting energy consumption, and (4) the back slashes represent the energy consumption of the spindle deceleration. The area size of the first scheme between the second scheme looks different. This shows that different cutting parameters cause different cutting and non-cutting energy consumption (Hu et al., 2019).

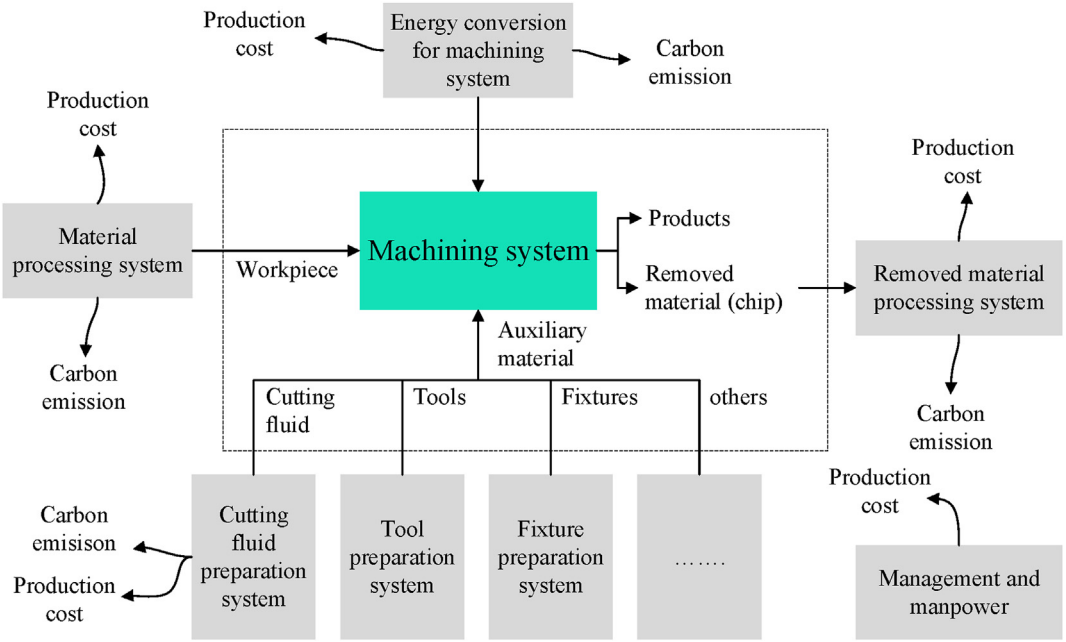

Figure 1. CNC turning system (adapted from Yi et al. (2015) with permission).

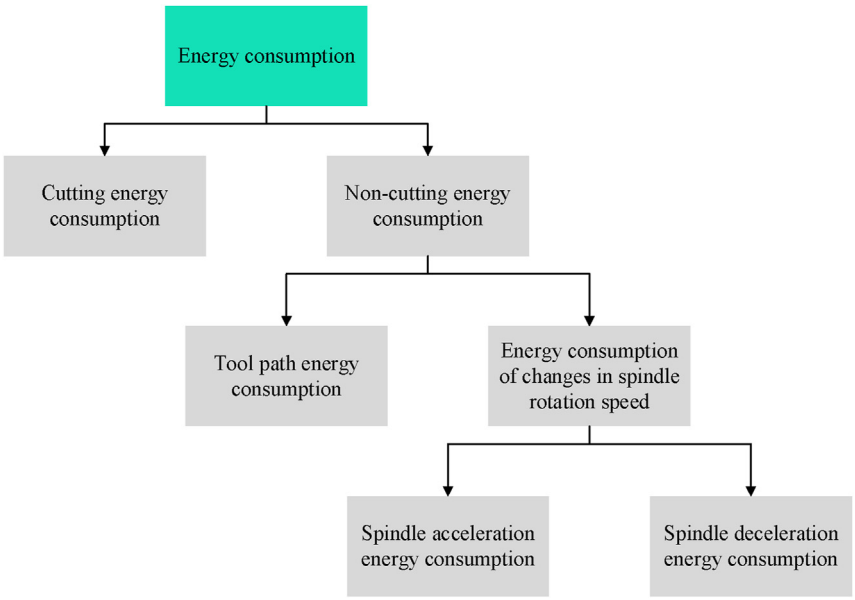

Figure 2. Energy consumption of CNC turning.

The spindle rotation speed in the first scheme was lower than that in the second scheme. This causes the cutting energy consumption in the first scheme to be greater than that in the second scheme because of the longer cutting time (Camposeco-Negrete, 2015). The second scheme is chosen as an energy-efficient option because it has a higher spindle rotation speed if only based on cutting energy consumption. However, the non-cutting energy consumption in the second scheme is greater than that in the first scheme because a high spindle rotation speed requires a high rotational change in energy consumption. If the high spindle rotation speed causes a decrease in the cutting energy consumption to fall behind the increment of the non-cutting energy consumption in the second scheme, then the first scheme will be a better option.

In a real manufacturing process, production time is also an important aspect in addition to energy consumption, carbon emission, and production costs. It is not reasonable to optimize these parameters by sacrificing the production time as this causes a machine tardiness problem (Hu et al., 2019). The production time is calculated based on the duration of power usage during the cutting and non-cutting processes, as shown in Figure 4.

Based on the aforementioned explanation, there are four objective functions considered in this research: energy consumption, carbon emissions, production time, and production costs. These objective functions are related to each other, as shown in Figure 5. As shown in the figure, production time is related to the other three aspects. Energy

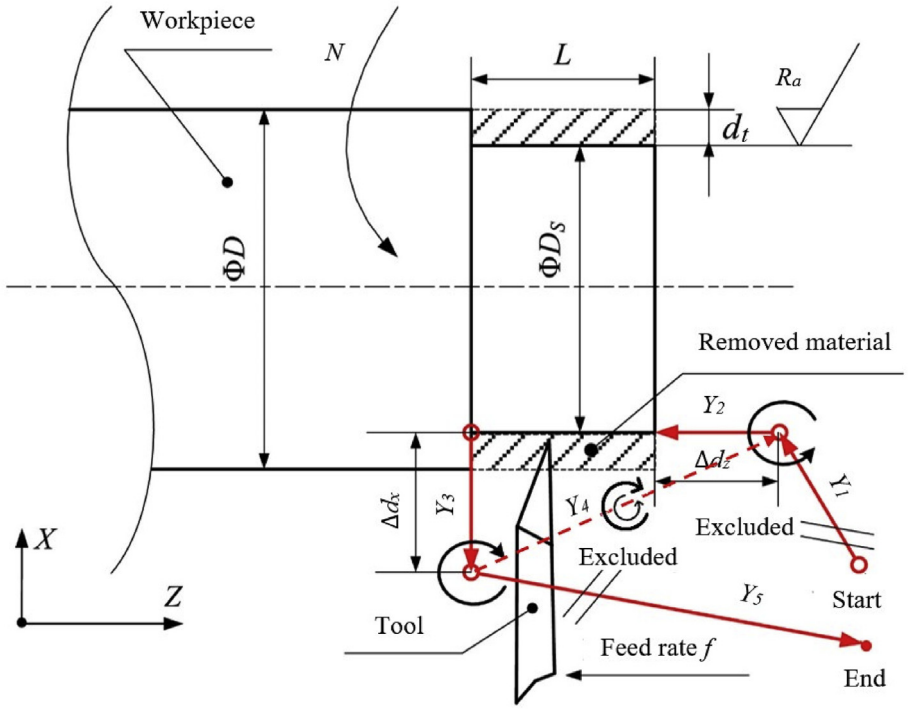

Figure 3. Multi-pass turning operations (adapted from Hu et al. (2019) with permission).

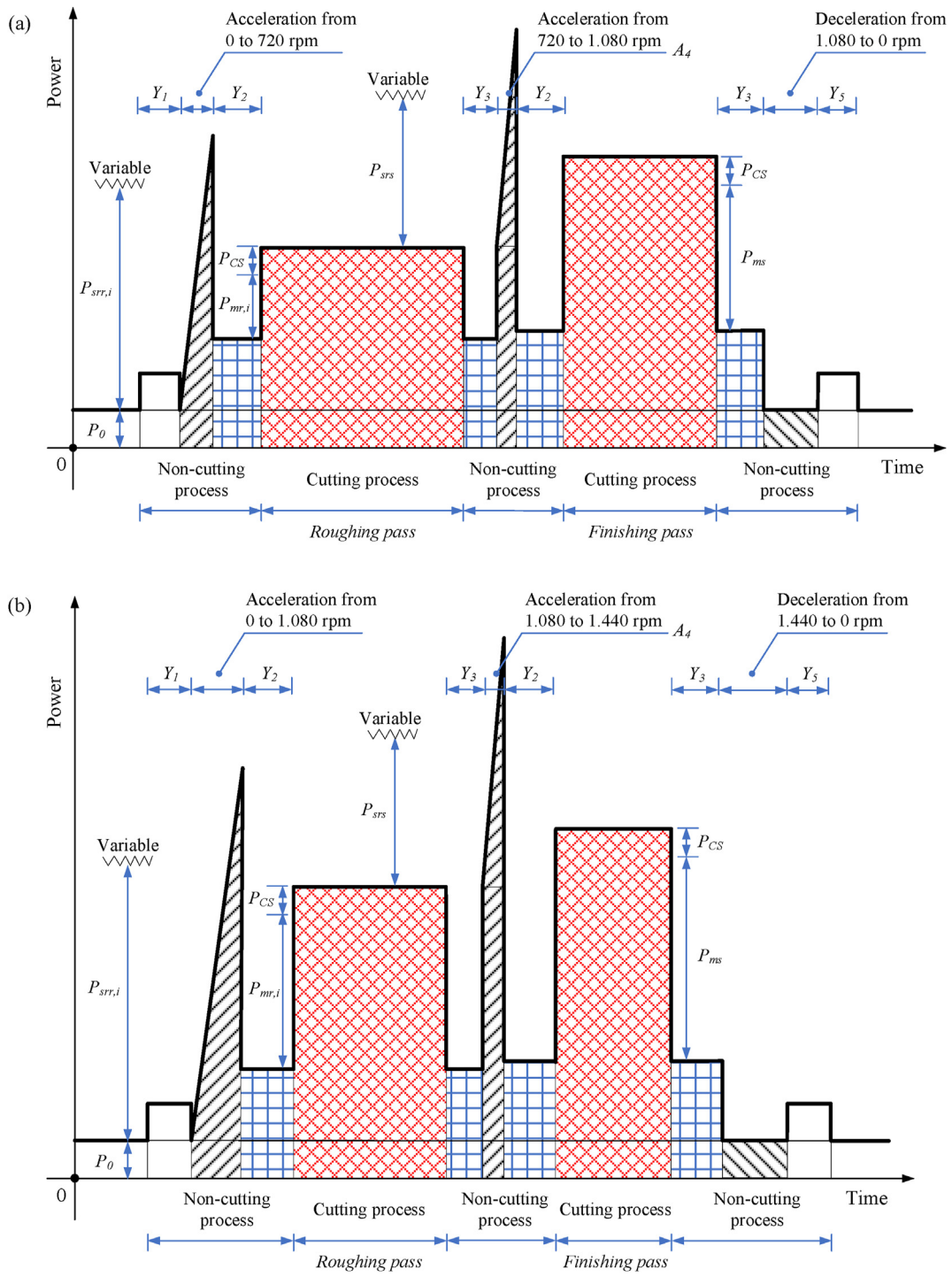

Figure 4. Power profiles of cutting parameter schemes (adapted from Hu et al. (2019) with permission).

consumption is one of the input components for carbon emissions and production costs. Each objective function can be converted to each other without the need to model four different objective functions. For example, production time can be converted into production costs in units of money per time. Even so, the minimum production time does not necessarily result in a minimum production cost, and vice versa because of the existence of the other objectives. However, each of the objective functions has its importance, which cannot be obtained by converting one objective function into another, so that each objective function needs to stand on its own.

3. Mathematical modeling

3.1. Objective functions

The objective functions of the model in this research are: (1) energy consumption, which refers to the model of Hu et al. (2019) and Lu et al. (2016); (2) carbon emission, which refers to the model of Yi et al. (2015); production cost, which refers to the model of Tian et al. (2019); and (4) production time, which refers to the model of Hu et al. (2019) and Lu et al. (2016).

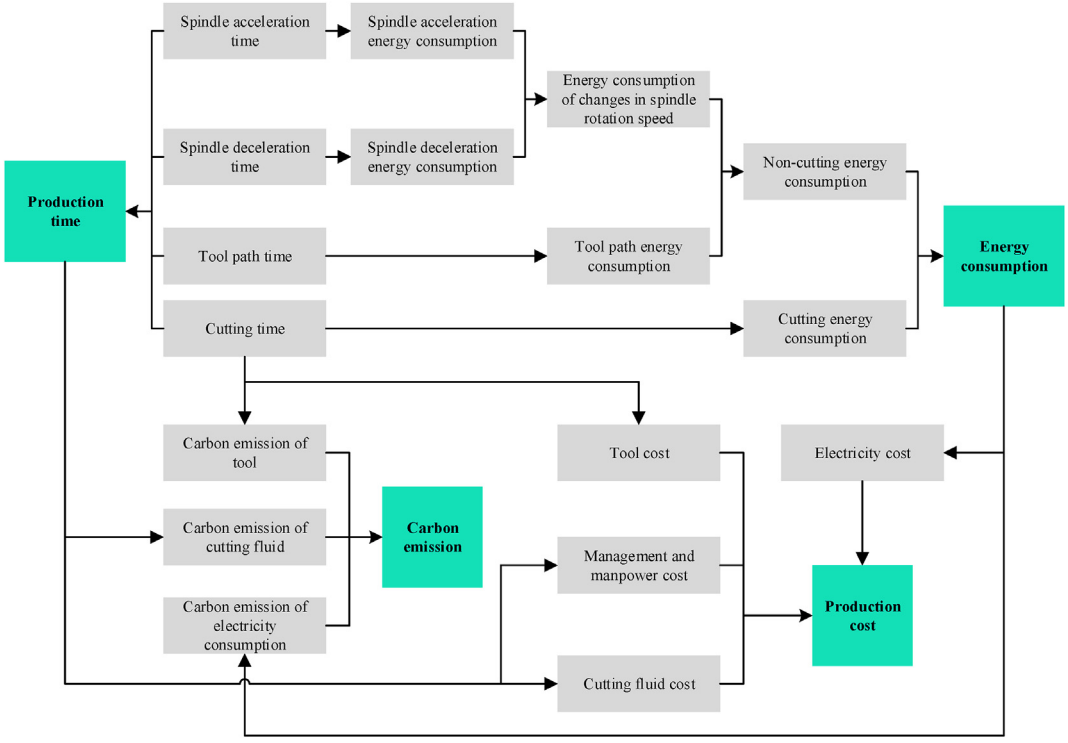

Figure 5. Integration flow of four aspects: energy consumption, carbon emission, production time, and production cost.

This optimization model aims to achieve minimum energy consumption, production time, carbon emissions, and production cost simultaneously. The decision variables consist of the spindle rotation speed for the *i*-th roughing pass and finishing pass, feed rate for the *i*-th roughing pass and finishing pass, depth of cut for the *i*-th roughing pass and finishing pass, and number of roughing passes. The objective functions can be expressed as

$$Minimize: F\left(N_{r,i}, N_s, f_{r,i}, f_s, d_{r,i}, d_s, n\right) = \left(\min E_{total}, \min T_{total}, \min CE_{total}, \min PC_{total}\right) \tag{1}$$

3.1.1. Energy consumption

The total energy consumption in the multi-pass turning is obtained from the cutting and non-cutting energy consumption (Hu et al., 2019). The total energy consumption is expressed as

$$E_{total} = E_{cut} + E_{non} \tag{2}$$

3.1.1.1. Cutting energy consumption. The cutting energy consumption consists of the energy consumption of standby, coolant spray, spindle rotation, *Z*-axial feeding, and material removal (Hu et al., 2019). This energy consumption is expressed as

$$E_{cut} = E_0 + E_{CS} + E_{SR} + E_{ZF} + E_{MC} \tag{3}$$

During the cutting process, the energy consumption in the multi-pass turning is generated from the temporal cutting power, which is assumed to be fixed.

In Eq. (3), the material removal was developed based on the machining energy consumption model of Lu et al. (2016). This model is divided into roughing and finishing passes. The material removal energy consumption is expressed as follows:

$$E_{MC} = P_{mr,i} \times t_{mr} + P_{ms} \times t_{ms} \tag{4}$$

The material removal power in the roughing and finishing passes (Chauhan et al., 2015) can be expressed as

$$P_{mr,i} = \frac{1000 k_f f_{r,i}^{\mu} d_{r,i}^{\vartheta} V_{r,i}}{6120\eta} \tag{5}$$

$$P_{ms} = \frac{1000 k_f f_s^{\mu} d_s^{\vartheta} V_s}{6120\eta} \tag{6}$$

In Eqs. (5) and (6), the cutting speed of the roughing and finishing passes can be calculated as follows:

$$V_{r,i} = \frac{\pi(D_i - d_{r,i})N_{r,i}}{1000} \tag{7}$$

$$V_s = \frac{\pi(D_{n+1} - d_s)N_s}{1000} \tag{8}$$

where $D_1 = D; D_i = D_{i-1} - 2d_{r,i-1}, i = \{2, \ldots, n\}$; and $D_{n+1} = D_n - 2d_{r,n}$.

The *Z*-axial feeding energy consumption in Eq. (3) can be expressed as

$$E_{ZF} = P_{zr,i} \times t_{mr} + P_{zs} \times t_{ms} \tag{9}$$

The *Z*-axial feeding power in the roughing and finishing passes is modeled with quadratic regression based on experimental data (Jia, 2014), which have a high degree of accuracy, as follows:

$$P_{zr,i} = A_{ZF}\left(N_{r,i} f_{r,i}\right)^2 + B_{ZF}\left(N_{r,i} f_{r,i}\right) + C_{ZF} \tag{10}$$

$$P_{zs} = A_{ZF}\left(N_s f_s\right)^2 + B_{ZF}\left(N_s f_s\right) + C_{ZF} \tag{11}$$

In Eq. (3), the spindle rotation energy consumption can be expressed as

$$E_{SR} = P_{sr,i} \times t_{mr} + P_{ss} \times t_{ms} \tag{12}$$

The spindle rotation power in the roughing and finishing passes is

modeled with quadratic regression based on experimental data (Lv et al., 2014), as follows:

$$P_{sr,i} = B_{SR}N_{r,i} + C_{SR} \tag{13}$$

$$P_{ss} = B_{SR}N_s + C_{SR} \tag{14}$$

Coolant spray energy consumption and standby energy consumption can be modeled as follows:

$$E_{CS} = P_{CS} \times T_{cut} \tag{15}$$

$$E_0 = P_0 \times T_{cut} \tag{16}$$

where P_{CS} and P_0 are the coolant spray power and standby power, respectively, as shown in Figure 4, which were obtained from the actual measurements (Hu et al., 2019).

In Eqs. (15) and (16), the cutting time (Chauhan et al., 2015; Shin and Joo, 1992) can be expressed as

$$T_{cut} = t_{mr} + t_{ms} \tag{17}$$

where

$$t_{mr} = \sum_{i=1}^{n} \frac{60\pi D_i L}{1000 V_{r,i} f_{r,i}} \tag{18}$$

$$t_{ms} = \frac{60\pi D_{n+1} L}{1000 V_s f_s} \tag{19}$$

3.1.1.2. Non-cutting energy consumption. Non-cutting energy consumption can be divided into three parts: tool path energy consumption, tool change energy consumption, and energy consumption of changes in spindle rotation speed (Hu et al., 2018). However, we assume that only one type of tool is used; hence, there is no tool to change the energy consumption in the model. The non-cutting energy consumption is expressed as

$$E_{non} = E_{TP} + E_{SRC} \tag{20}$$

In Figure 3, there are five feeding activities during multi-pass turning. The first and fifth feeding activities do not have to be modeled because they are rapidly feeding. The fourth feeding activity pertains to changes in the spindle rotation speed. Consequently, the tool-path energy consumption can be expressed as

$$E_{TP} = E_{TP}^2 + E_{TP}^3 \tag{21}$$

The second feeding activity uses the spindle rotation speed, and the feed direction is *Z*-axial. The tool path energy consumption in the second feeding activity is modeled as follows:

$$E_{TP}^2 = P_0(t_2) + (P_{sr,i} + P_{zr,i})t_{2r,i} + (P_{ss} + P_{zs})t_{2s} \tag{22}$$

The time required for the second feeding activity is expressed as

$$t_2 = t_{2r,i} + t_{2s} \tag{23}$$

where

$$t_{2r,i} = \sum_{i=1}^{n} \frac{60\Delta d_z}{N_{r,i} f_{r,i}} \tag{24}$$

$$t_{2s} = \frac{60\Delta d_z}{N_s f_s} \tag{25}$$

The third feeding activity uses the spindle rotation speed that takes place quickly, and the feed direction is *X*-axial. The tool path energy consumption in the third feeding activity is modeled as follows:

$$E_{TP}^3 = (P_0 + P_{XR})t_3 + P_{sr,i}(t_{3r,i}) + P_{ss}(t_{3s}) \tag{26}$$

The time required for the third feeding activity is expressed as

$$t_3 = t_{3r,i} + t_{3s} \tag{27}$$

where

$$t_{3r,i} = \sum_{i=1}^{n} \frac{60(\Delta d_x + d_{r,i})}{1000 v_{XR}} \tag{28}$$

$$t_{3s} = \frac{60(\Delta d_x + d_s)}{1000 v_{XR}} \tag{29}$$

In multi-pass turning, spindle rotation speed undergoes: (1) acceleration from 0 rpm to $N_{r,1}$ rpm; (2) acceleration or deceleration from $N_{r,1}$ rpm to $N_{r,i+1}$ rpm and from $N_{r,n}$ rpm to N_s rpm; and (3) deceleration from N_s rpm to 0 rpm. Consequently, the energy consumption of the spindle rotation speed is expressed as

$$E_{SRC} = E_{sra} + E_{srm} + E_{srd} \tag{30}$$

The energy consumption, power, and time required for acceleration from 0 rpm to $N_{r,1}$ rpm are expressed in Eqs. (31), (32), and (33), respectively.

$$E_{sra} = \int_0^{t_{sra}} (P_0 + P_{sra})dt \tag{31}$$

$$P_{sra} = B_{SR} \times \left(\frac{30\alpha_A t}{\pi}\right) + C_{SR} + T_A \times (\alpha_A t) \tag{32}$$

$$t_{sra} = \frac{2\pi N_{r,1}}{60\alpha_A} \tag{33}$$

The energy consumption, power, and time required for acceleration or deceleration from $N_{r,1}$ rpm to $N_{r,i+1}$ rpm and from $N_{r,n}$ rpm to N_s rpm (Hu et al., 2017) are expressed in Eqs. (34), (35), (36), (37), (38), and (39).

$$E_{srm} = \int_0^{t_{srm}} (P_0)dt + \int_0^{t_{srr,i}} (P_{srr,i})dt + \int_0^{t_{srs}} (P_{srs})dt \tag{34}$$

$$P_{srr,i} = \begin{cases} B_{SR} \times \left(N_{r,i-1} + \frac{30\alpha_A t}{\pi}\right) + C_{SR} + T_A \times \left(\frac{\pi N_{r,i-1}}{30} + \alpha_A t\right), if N_{r,i} > N_{r,i-1} \\ 0, if N_{r,i} < N_{r,i-1} \end{cases} \tag{35}$$

$$P_{srs} = \begin{cases} B_{SR} \times \left(N_{r,n} + \frac{30\alpha_A t}{\pi}\right) + C_{SR} + T_A \times \left(\frac{\pi N_{r,n}}{30} + \alpha_A t\right), if N_s > N_{r,n} \\ 0, if N_s < N_{r,n} \end{cases} \tag{36}$$

$$t_{srm} = t_{srr,i} + t_{srs} \tag{37}$$

$$t_{srr,i} = \sum_{i=2}^{n} \begin{cases} \frac{2\pi(N_{r,i} - N_{r,i-1})}{60\alpha_A}, if N_{r,i} > N_{r,i-1} \\ \frac{2\pi(N_{r,i} - N_{r,i-1})}{60\alpha_D}, if N_{r,i} < N_{r,i-1} \end{cases} \tag{38}$$

$$t_{srs} = \begin{cases} \frac{2\pi(N_s - N_{r,n})}{60\alpha_A}, \ if N_s > N_{r,n} \\ \frac{2\pi(N_s - N_{r,n})}{60\alpha_D}, \ if N_s < N_{r,n} \end{cases} \tag{39}$$

where $i = \{2, \ldots, n\}$.

The energy consumption for spindle deceleration from N_s rpm to 0 rpm normally consumes standby power (Hu et al., 2017). Hence, it can be expressed as

$$E_{srd} = P_0 \times t_{srd} \tag{40}$$

where the time required for that can be expressed as

$$t_{srd} = \frac{-2\pi N_s}{60\alpha_D} \tag{41}$$

3.1.2. Production time

Similar to energy consumption, the production time is obtained from the cutting and non-cutting production times (Hu et al., 2019). Based on Eqs. (18), (19), (24), (25), (28), (29), (33), (38), (39), and (40), the production time for multi-pass turning can be calculated by

$$T_{total} = t_{mr} + t_{ms} + t_{2r,i} + t_{2s} + t_{3r,i} + t_{3s} + t_{sra} + t_{srr,i} + t_{srs} + t_{srd} = \sum_{i=1}^{n} \frac{60\pi D_i L}{1000 V_{r,i} f_{r,i}} + \frac{60\pi D_{n+1} L}{1000 V_s f_s} + \sum_{i=1}^{n} \frac{60\Delta d_z}{N_{r,i} f_{r,i}} + \frac{60\Delta d_z}{N_s f_s} + \sum_{i=1}^{n} \frac{60(\Delta d_x + d_{r,i})}{1000 v_{XR}} + \frac{60(\Delta d_x + d_s)}{1000 v_{XR}} + \frac{2\pi N_{r,1}}{60\alpha_A} + \sum_{i=2}^{n} \begin{cases} \frac{2\pi(N_{r,i} - N_{r,i-1})}{60\alpha_A}, if N_{r,i} > N_{r,i-1} \\ \frac{2\pi(N_{r,i} - N_{r,i-1})}{60\alpha_D}, if N_{r,i} < N_{r,i-1} \end{cases} + \begin{cases} \frac{2\pi(N_s - N_{r,n})}{60\alpha_A}, if N_s > N_{r,n} \\ \frac{2\pi(N_s - N_{r,n})}{60\alpha_D}, if N_s < N_{r,n} \end{cases} + \frac{-2\pi N_s}{60\alpha_D} \tag{42}$$

In Eq. (42), there is a condition in which the spindle can experience acceleration or deceleration. If the current spindle rotation speed is higher than the previous one, then the calculation of the change time of the spindle rotation speed uses the spindle angular acceleration α_A. If the current spindle rotation speed is lower than the previous one, the calculation of the change time of the spindle rotation speed uses the spindle angular deceleration α_D.

3.1.3. Carbon emissions

Carbon emissions in CNC turning systems, which are affected by cutting parameters, are the carbon emissions generated from electricity consumption, tools, and cutting fluids (Yi et al., 2015). Carbon emissions in multi-pass turning can be calculated by

$$CE_{total} = CE_{elec} + CE_{tool} + CE_{fluid} \tag{43}$$

In Eq. (43), the carbon emissions from electricity consumption have a linear relationship with the carbon emission factor and the total energy consumption during the turning process. It can be expressed as

$$CE_{elec} = CEF_{elec} \times E_{total} \tag{44}$$

where the carbon emission factor for electricity consumption is adopted from the National Development and Reform Commission of China (2013).

Carbon emissions generated from a tool can be obtained by multiplying the weight of the cutting time of the tool's life by the total carbon emissions during its lifecycle. The carbon emissions are calculated as follows:

$$CE_{tool} = \frac{T_{cut}}{(R+1)T_p} \times CEF_{tool} \times M_{tool} \tag{45}$$

The tool life can be estimated from Taylor's tool life equation. This can be extended by inputting the cutting parameters in the multi-pass turning (Bagaber and Yusoff, 2019). The tool life is expressed as (Chen and Tsai, 1996; Onwubolu and Kumalo, 2001)

$$T_p = \theta T_r + (1-\theta) T_s \tag{46}$$

where

$$T_r = \sum_{i=1}^{n} \frac{60 C_O}{V_{r,i}^p f_{r,i}^q d_{r,i}^r} \tag{47}$$

$$T_s = \frac{60 C_O}{V_s^p f_s^q d_s^r} \tag{48}$$

As shown in Eq. (43), the total carbon emissions consist of carbon emissions resulting from the use of energy, tools, and fluids. Two of them are fully expressed as functions of other objective functions, namely total energy consumption and total production time. Hence, only the tool's carbon emissions could make the trade-off towards other objective functions. The tool's carbon emissions move in the opposite direction toward power energy consumption. As shown in Eqs. (18) and (19), the decision variables become the denominators of the components of T_{cut}, whereas in Eqs. (5) and (6), the decision variables become the nominators of the power energy consumption. The higher the value of the decision variables, the lower the tool's carbon emissions will be, while at the same time, it will increase the power energy consumption. Hence, there is a trade-off between energy consumption and carbon emissions. This trade-off will make another trade-off between the rest of the objective functions because they affect each other, as shown earlier in Figure 5.

The carbon emissions of the cutting fluid in Eq. (43) can be obtained by multiplying the weight of the production time of the cutting fluid's lifetime by the total carbon emission of the cutting fluid during its lifecycle. Generally, cutting fluids can be divided into two types: water- and oil-based cutting fluids (Yi et al., 2015). In this research, we assume that only water-based cutting fluids are used. The carbon emissions of the cutting fluid are expressed as

$$CE_{fluid} = \frac{T_{total}}{2.592.000 T_{fluid}} \times \left[CEF_{oil} \times (V_{in} + V_{ad}) + CEF_{wc} \times \frac{(V_{in} + V_{ad})}{\delta_f} \right] \tag{49}$$

3.1.4. Production cost

The production cost considered in this research consists of electricity, tool, cutting fluid, and management and manpower costs, which can be expressed as (Tian et al., 2019)

$$PC_{total} = PC_{elec} + PC_{tool} + PC_{fluid} + PC_m \tag{50}$$

The electricity, tool, cutting fluid, management, and manpower costs are expressed in Eqs. (51), (52), (53), and (54), as follows:

$$PC_{elec} = E_{total} \times C_{elec} \tag{51}$$

$$PC_{tool} = \frac{T_{cut}}{(R+1)T_p} \times C_{tool} \times M_{tool} \tag{52}$$

$$PC_{fluid} = \frac{T_{total}}{2.592.000 T_{fluid}} \times (V_{in} + V_{ad}) \times C_{fluid} \tag{53}$$

$$PC_m = T_{total} \times C_m \tag{54}$$

3.2. Constraints

The optimal cutting parameters should satisfy several constraints imposed in the model, i.e., cutting parameters, tool life, cutting force,

power, chip-tool interface temperature, stable cutting region, surface roughness, and parameter relations.

3.2.1. Cutting parameters constraint

This constraint serves as the solution space of the model and is expressed as the range value of the spindle rotation speed, feed rate, and depth of cut in the form of lower and upper bounds. The range largely depends on the type of tool, machine, and workpiece material. These constraints are expressed as follows:

$$d_{rL} \le d_{r,i} \le d_{rU} \tag{55}$$

$$d_{sL} \le d_s \le d_{sU} \tag{56}$$

$$f_{rL} \le f_{r,i} \le f_{rU} \tag{57}$$

$$f_{sL} \le f_s \le f_{sU} \tag{58}$$

$$\frac{1000V_{rL}}{\pi(D_i - d_{r,i})} \le N_{r,i} \le N_{max} \tag{59}$$

$$\frac{1000V_{sL}}{\pi(D_{n+1} - d_s)} \le N_s \le N_{max} \tag{60}$$

3.2.2. Tool-life constraint

This constraint is required to achieve economical production and quality of the processed components. The minimum value of the tool life should not be less than the length of the cutting time for machining one workpiece. Likewise, the maximum value of the tool life should not exceed the length of the cutting time for machining one workpiece. These constraints are expressed as follows:

$$T_L \le T_r \le T_U \tag{61}$$

$$T_L \le T_s \le T_U \tag{62}$$

3.2.3. Cutting force constraint

This constraint is needed to avoid the excessive deflection of workpieces and tools and to avoid tool damage, which can result in dimensional errors. These constraints are expressed as follows:

$$F_{r,i} = k_f f_{r,i}^{\mu} d_{r,i}^{\vartheta} \le F_U \tag{63}$$

$$F_s = k_f f_s^{\mu} d_s^{\vartheta} \le F_U \tag{64}$$

3.2.4. Power constraint

The power required during multi-pass turning should not exceed the maximum power of the machine. These constraints are expressed as follows:

$$P_{r,i} = P_{mr,i} + P_{zr,i} + P_{sr,i} + P_{CS} + P_0 \le P_U \tag{65}$$

$$P_s = P_{ms} + P_{zs} + P_{ss} + P_{CS} + P_0 \le P_U \tag{66}$$

3.2.5. Chip-tool interface temperature constraint

The tool life is strongly influenced by the chip-tool interface temperature. As the sharpness and hardness decrease, the tool can no longer be used to cut if the temperature exceeds the limit. These constraints are expressed as follows:

$$Q_{r,i} = k_q V_{r,i}^{\tau} f_{r,i}^{\varphi} d_{r,i}^{\delta} \le Q_U \tag{67}$$

$$Q_s = k_q V_s^{\tau} f_s^{\varphi} d_s^{\delta} \le Q_U \tag{68}$$

3.2.6. Stable cutting region constraint

This constraint is required to prevent chatter vibration, adhesion, and built-up edge formation. The stable cutting region should be larger than a certain area. These constraints are expressed as follows:

$$S_{r,i} = V_{r,i}^{\lambda} f_{r,i} d_{r,i}^{v} \ge Sc \tag{69}$$

$$S_s = V_s^{\lambda} f_s d_s^{v} \ge Sc \tag{70}$$

3.2.7. Surface roughness constraint

The surface roughness represents the quality of a workpiece and is commonly influenced by the cutting speed and nose radius of the tool. Generally, the surface roughness should be less than a specified value. This constraint is expressed as follows:

$$\frac{f_s^2}{8R_n} \le R_a \tag{71}$$

3.2.8. Parameter relations constraints

The depth of cut and feed rate in the roughing pass are usually greater than those in the finishing pass. However, the cutting speed in the roughing pass is typically smaller than that in the finishing pass. In addition, the depth of the removed material must be equal to the sum of the cutting depth, i.e., the number of n depths of cut at the roughing pass and one depth of cut at the finishing pass. The value of n is the number of integers. These constraints are expressed as follows:

$$V_s > k_1 V_{r,i} \tag{72}$$

$$f_{r,i} > k_2 f_s \tag{73}$$

$$d_{r,i} > k_3 d_s \tag{74}$$

$$d_t = d_s + \sum_{i=1}^{n} d_{r,i} \tag{75}$$

$$n_L \le n \le n_U, and integer \tag{76}$$

4. Numerical example

The data used in the numerical example were taken from Bagaber and Yusoff (2019), Hu et al. (2019), Lu et al. (2016), Tian et al. (2019), and Yi et al. (2015).

4.1. Model parameters

A workpiece of C45 carbon steel forging bar with a diameter D and length L of 80 mm and 200 mm, respectively, was processed with cutting speeds from 50 to 500 m/min. This steel has a yield strength of 305 N/mm^2, tensile strength of 580 N/mm^2, and hardness of 84 HRC (Bringas, 2004). Table 2 lists the tool specifications used during turning. During its life cycle, the tool is assumed to be sharpened (R) 10 times.

The machining process uses wet cutting with a coolant spray turned on. This process uses a water-based cutting fluid with a concentration δ_f of 0.05. The initial V_{in} and additional V_{ad} volumes of cutting fluid used were 8.5 × 10–3 m^3 and 4.5 × 10–3 m^3, respectively. The cutting fluid replacement cycle T_{fluid} lasted for 2 months.

The energy consumption, carbon emissions, and production cost parameters are shown in Tables 3, 4, and 5, respectively. The coefficients and constants associated with the machining conditions are shown in Table 6. The constraints are presented in Table 7.

Table 2. Tool specifications.

Parameter	Notation (Unit)	Value
Inclination angle	(°)	5
Tool lead angle	(°)	45
Rake angle	(°)	20
Hardness	(HRC)	69–81
Nose radius	R_n (mm)	1.2
Mass	M_{tool} (kg)	0.015

Table 3. Parameters of energy consumption.

Parameter	Notation (Unit)	Value
Spindle angular acceleration	α_A (rad/s^2)	39.78
Spindle angular deceleration	α_D (rad/s^2)	-38.79
Spindle acceleration torque	T_A (N.m)	28.42
Standby power	P_0 (W)	332.1
Coolant spray power	P_{CS} (W)	369.5
X-axis rapid feeding power	P_{XR} (W)	135
X-axis rapid feeding speed	v_{XR} (m/min)	4
X-axis retracting distance	Δd_x (mm)	2.1
Z-axial air-cutting distance	Δd_z (mm)	5
Power efficiency	η	0.85

4.2. Optimization

There are several steps to find the optimal solution for multi-objective optimization (Marler & Arora, 2004, 2005), i.e., (1) determination of the minimum and maximum solutions of the objective function, (2) normalization of the objective function, (3) weighting of the objective function, and (4) solving the multi-objective optimizations.

4.2.1. Determination of the minimum and maximum values

The model was solved using the OptQuest tool in the Oracle Crystal Ball software. This software uses an advanced optimization feature with multiple complementary search methodologies, including advanced Tabu search and scatter search (Rosyidi et al., 2020). The model was solved by 10,000 iterations to obtain the optimal solutions for both minimum and maximum values. Before that, the decision variable of the number of roughing passes (n) needs to be determined in advance in this model. Minimum and maximum solutions are obtained from the smallest and largest n values by considering the depth of the cut constraints $\left(n = \frac{d_t - d_{sU}}{d_{rU}} \geq n_L and n = \frac{d_t - d_{sL}}{d_{rL}} \leq n_U\right)$. In multi-pass turning, there are n roughing passes and one finishing pass. Therefore, the feasible minimum and maximum solutions are obtained if the values of n are 3 and 7, respectively. The optimal solutions for each objective function are listed in Table 8.

4.2.2. Normalization

A function transformation (normalization) is necessary to combine all the objective functions and establish a nondimensional objective function. The function transformation of each objective function is expressed as follows:

$$F^{trans}_{E_{total}} = \frac{E_{total} - 2,923,482.00}{8,767,189.88 - 2,923,482.00} = \frac{E_{total} - 2,923,482.00}{5,843,707.88} \quad (77)$$

$$F^{trans}_{T_{total}} = \frac{T_{total} - 619.26}{1,204.55 - 619.26} = \frac{T_{total} - 619.26}{585.29} \quad (78)$$

$$F^{trans}_{CE_{total}} = \frac{CE_{total} - 0.67}{1.98 - 0.67} = \frac{CE_{total} - 0.67}{1.31} \quad (79)$$

$$F^{trans}_{PC_{total}} = \frac{PC_{total} - 17,515.39}{33,921.29 - 17,515.39} = \frac{PC_{total} - 17,515.39}{16,405.91} \quad (80)$$

4.2.3. Weighting

In this research, we use the weighted sum method and assume that each objective function is given the same weight. Therefore, the objective function of the multi-objective optimization in this model is expressed as

$$U = 0,25 \times \left(F^{trans}_{E_{total}} + F^{trans}_{T_{total}} + F^{trans}_{CE_{total}} + F^{trans}_{PC_{total}}\right) \quad (81)$$

4.2.4. Optimization results

Eq. (81) becomes the objective function of the model, and Eqs. (55), (56), (57), (58), (59), (60), (61), (62), (63), (64), (65), (66), (67), (68), (69), (70), (71), (72), (73), (74), (75), and (76) constitute the constraints. Figure 6 shows the Pareto front of the objective functions. The plot was obtained using the *gamultiobj* function of Matlab R2020b, which according to Garcia and Trinh (2019), is an implementation of the non-dominated sorting genetic algorithm. This function has been used in many multi-objective optimizations of machining parameter papers and other related fields, such as Gaudencio et al. (2019), Garcia and Trinh (2019), and Sada (2020). Figure 6(a) shows the trade-off between carbon emissions and production time, Figure 6(c) shows the trade-off between production cost and production time, Figure 6(d) shows the trade-off between carbon emissions and energy consumption, and Figure 6(e) shows the trade-off between production cost and energy consumption. The result in Figure 6(a) agrees with the Pareto front in the research of Liu et al. (2016), and the result in Figure 6(b) agrees with the Pareto front in the research of He et al. (2017).

Figure 6(b) and 6(f) show that there are no trade-offs between energy consumption and production time and between production cost and carbon emissions. For energy consumption and production time, the results can be traced from the equations that determine both objectives. The energy consumption was expressed as a function of production time, and the production time was calculated based on the time that is the multiplier of the energy consumption. For the production cost and carbon emission, there was no trade-off because both objectives have two common components in terms of electrical energy and total time. In each case, whenever one objective function increases, the other objective function will also increase, and vice versa. These results are consistent with the results of several studies in which trade-offs were not found for all objectives. According to Henig and Buchanan (1997), trade-offs are typically found in multi-objective optimization. Awad and Khanna (2015) implied that, in a few cases, no trade-offs were found between the

Table 4. Parameters of carbon emission.

Parameter	Notation (Unit)	Value
Carbon emission factor of electricity consumption	CEF_{elec} (kgCO_2/J)	2.25×10^{-7}
Carbon emission factor of tool	CEF_{tool} (kgCO_2/kg)	31.5
Carbon emission factor of soluble oil	CEF_{oil} (kgCO_2/m^3)	500
Carbon emission factor of waste liquid	CEF_{wc} (kgCO_2/m^3)	200

Table 5. Parameters of production cost.

Parameter	Notation (Unit)	Value
Coefficient of electricity cost	C_{elec} (IDR/J)	0.00528
Coefficient of tool cost	C_{tool} (IDR/kg)	11,000
Coefficient of cutting fluid cost	C_{fluid} (IDR/m^3)	290,000,000
Coefficient of management and manpower cost	C_m (IDR/s)	23.61

Table 6. Coefficients and constants associated to machining condition.

Parameter	Notation	Value
Monomial coefficient of spindle rotation power	B_{SR}	1.09
Constant of spindle rotation power	C_{SR}	41.12
Quadratic coefficient of *Z*-axial feeding power	A_{ZF}	2.32×10^{-6}
Monomial coefficient of *Z*-axial feeding power	B_{ZF}	0.03
Constant of *Z*-axial feeding power	C_{ZF}	0.49
Coefficient of tool-workpiece combination	k_f	108
Weighted coefficient of tool-life	θ	0.5
Coefficient associated to tool-life equation	C_O	6×10^{11}
Constant associated to tool-life equation	p	5
Constant associated to tool-life equation	q	1.75
Constant associated to tool-life equation	r	0.75
Constant associated to cutting force and power model	μ	0.75
Constant associated to cutting force and power model	ϑ	0.95
Constant associated to stable cutting region model	λ	2
Constant associated to stable cutting region model	ν	-1
Coefficient associated to chip-tool interface temperature model	k_q	132
Constant associated to chip-tool interface temperature model	δ	0.105
Constant associated to chip-tool interface temperature model	τ	0.4
Constant associated to chip-tool interface temperature model	φ	0.2
Relation constant of roughing passes and finishing pass	k_1	1
Relation constant of roughing passes and finishing pass	k_2	2.5
Relation constant of roughing passes and finishing pass	k_3	1

Table 7. Constraints.

Parameter	Notation (Unit)	Value
Minimum depth of cut for roughing pass	d_{rL} (mm)	1
Maximum depth of cut for roughing pass	d_{rU} (mm)	3
Minimum depth of cut for finishing pass	d_{sL} (mm)	1
Maximum depth of cut for finishing pass	d_{sU} (mm)	3
Total depth of removed material	d_t (mm)	10
Minimum feed rate for roughing pass	f_{rL} (mm/rev)	0.1
Maximum feed rate for roughing pass	f_{rU} (mm/rev)	0.9
Minimum feed rate for finishing pass	f_{sL} (mm/rev)	0.1
Maximum feed rate for finishing pass	f_{sU} (mm/rev)	0.9
Maximum cutting force	F_U (kgf)	4,903.325
Minimum number of roughing passes	n_L	1
Maximum number of roughing passes	n_U	7
Maximum spindle rotation speed	N_{max} (rpm)	2,000
Maximum power	P_U (W)	7,500
Maximum temperature	Q_U (°C)	1,000
Maximum surface roughness	R_a (mm)	6.3
Stable cutting region bound	Sc	140
Minimum tool-life	T_L (s)	1,500
Maximum tool-life	T_U (s)	2,700
Minimum cutting speed for roughing pass	V_{rL} (m/min)	50
Maximum cutting speed for roughing pass	V_{rU} (m/min)	500
Minimum cutting speed for finishing pass	V_{sL} (m/min)	50
Maximum cutting speed for finishing pass	V_{sU} (m/min)	500

objectives. Hence, trade-offs may exist in some objectives, and there are no trade-offs among the others. He et al. (2017) showed that among the three objectives involved in the model, no trade-off was found in one out of three objective combinations. We can find similar results in the multi-objective optimization models of Rao et al. (2017) and Ashbolt et al. (2017). Even in the latter research, the relationship between objectives with no trade-offs is linear and exponential.

The results of the multi-objective optimization are listed in Table 9. The value of the objective function is 0.0946 with a total energy consumption of 3,143,778.23 J, total production time of 729.14 s, total

Table 8. Optimization solutions of each objective function.

Decision variable	E_{total} (J)		T_{total} (s)		CE_{total} ($kgCO_2$)		PC_{total} (Rp)	
	Minimum	Maximum	Minimum	Maximum	Minimum	Maximum	Minimum	Maximum
$N_{r,1}$ (rpm)	270.08	291.77	276.38	302.94	270.08	300.38	277.60	299.45
$N_{r,2}$ (rpm)	305.67	334.89	300.36	338.33	305.67	333.67	291.20	329.77
$N_{r,3}$ (rpm)	330.57	284.72	298.69	273.93	330.57	275.28	325.00	276.89
$N_{r,4}$ (rpm)	-	355.26	-	331.93	-	354.83	-	364.00
$N_{r,5}$ (rpm)	-	347.62	-	370.87	-	367.21	-	372.18
$N_{r,6}$ (rpm)	-	391.72	-	361.39	-	362.80	-	368.20
$N_{r,7}$ (rpm)	-	389.12	-	390.33	-	389.98	-	387.14
$f_{r,1}$ (mm/rev)	0.34	0.29	0.31	0.28	0.34	0.28	0.30	0.28
$f_{r,2}$ (mm/rev)	0.30	0.25	0.31	0.25	0.30	0.25	0.30	0.25
$f_{r,3}$ (mm/rev)	0.30	0.25	0.32	0.28	0.30	0.28	0.30	0.28
$f_{r,4}$ (mm/rev)	-	0.25	-	0.29	-	0.25	-	0.25
$f_{r,5}$ (mm/rev)	-	0.28	-	0.25	-	0.25	-	0.25
$f_{r,6}$ (mm/rev)	-	0.25	-	0.29	-	0.29	-	0.29
$f_{r,7}$ (mm/rev)	-	0.25	-	0.25	-	0.25	-	0.25
$d_{r,1}$ (mm)	2.50	1.03	3.00	1.00	2.50	1.06	2.50	1.03
$d_{r,2}$ (mm)	2.50	1.03	2.94	1.00	2.50	1.03	2.50	1.03
$d_{r,3}$ (mm)	2.51	2.83	3.00	3.00	2.50	2.81	2.50	2.82
$d_{r,4}$ (mm)	-	1.03	-	1.00	-	1.03	-	1.03
$d_{r,5}$ (mm)	-	1.03	-	1.00	-	1.03	-	1.03
$d_{r,6}$ (mm)	-	1.03	-	1.00	-	1.03	-	1.03
$d_{r,7}$ (mm)	-	1.03	-	1.00	-	1.03	-	1.03
N_s (rpm)	478.87	575.45	505.59	549.58	466.59	548.22	475.60	569.64
f_s (mm/rev)	0.12	0.10	0.13	0.10	0.12	0.10	0.12	0.10
d_s (mm)	2.50	1.00	1.06	1.00	2.50	1.00	2.50	1.00
Value	2,923,482.00	8,767,189.88	619.26	1,204.55	0.67	1.98	17,515.39	33,921.29

carbon emission of 0.72 $kgCO_2$, and total production cost of IDR 19,405.45. To assess the sustainability performance of these results, an evaluation index is required. According to Sihag and Sangwan (2019), the sustainability assessment index (SAI) can be calculated by summing all the normalized and weighted indicators. Because the objective function is minimized, the calculation of the SAI is $1 - U$. As a result, the SAI for this numerical example is 0.9054, which means that the sustainability performance of the optimum solution is 90.54%.

4.3. Sensitivity analysis

Bagaber and Yusoff (2019), Lu et al. (2016), and Yi et al. (2015) conducted experiments to understand the relationship between the cutting parameters and objective functions. In this research, sensitivity analysis is carried out to study the behavior of the model toward changes in some model parameters (i.e., $N_{r,i}$,N_s,$f_{r,i}$,f_s,$d_{r,i}$,d_s,*and* n) in terms of the value of the objective functions (i.e., E_{total}, T_{total}, CE_{total} *and* PC_{total}). All decision variables were chosen as control parameters, where n was equal to 3. Various sets of experiments were designed for the analysis. The values of the control parameters are listed in Table 10, where they cover a feasible range. These experiments were divided into seven configurations: (1) $N_{r,1}$ and $f_{r,1}$, (2) $N_{r,2}$ and $f_{r,2}$, (3) $N_{r,3}$ and $f_{r,3}$, (4) N_s and f_s, (5) $d_{r,1}$ and d_s, (6) $d_{r,2}$ and d_s, and (7) $d_{r,3}$ and d_s.

The first configuration was tested with 16 combinations, and the results are shown in Figure 7. This figure shows that different settings of feed rate and spindle rotation speed have significant effects on energy consumption, production time, carbon emission, and production cost. Each objective function decreases as the feed rate and spindle rotation speed increase. A high spindle rotation speed causes the cutting force to decrease. This is caused by the workpiece, which has less time to deform at the cutting region. A higher spindle rotation speed leads to a reduction in energy consumption and carbon emissions. In contrast to the feed rate, there are two conflicting factors. An increased feed rate causes the cutting force to increase as well, but the production time is decreased because the time needed to remove the material is reduced. Nevertheless, a high feed rate still results in low energy consumption and carbon emissions, which is similar to that found by Yi et al. (2015) and Yin et al. (2019). As the production time decreases, the production costs generated during the turning process also decrease. Additionally, a large amount of energy consumption increases production costs. Therefore, energy consumption and production costs are kept at a minimum to achieve sustainable manufacturing. Similar results of sensitivity analysis can be observed in the second to fourth configurations. This implies that the parameters ($N_{r,i}$, $f_{r,i}$, N_s and f_s) are sensitive to the objective functions (E_{total}, T_{total}, CE_{total}, *and* PC_{total}).

The fifth configuration was tested with four combinations, and the results are shown in Figure 8. In this analysis, the combinations of the depth of cut for the roughing pass $d_{r,i}$ and finishing pass d_s should satisfy Eq. (75), the sum of which equals the total depth of the workpiece to be removed. For instance, if the value of $d_{r,1}$ is 2.51 mm, then d_s is 2.49 mm. Another depth of cut ($d_{r,2}$ and $d_{r,3}$) are control parameters, each of which is 0.25 mm. Figure 8 reveals that the depth of cut has little influence on energy consumption, production time, carbon emissions, and production costs. This implies that the depth of the cut is not sensitive to the objective functions. The three objectives increased slightly when the depth of cut increased. However, a different observation from Figure 8 is

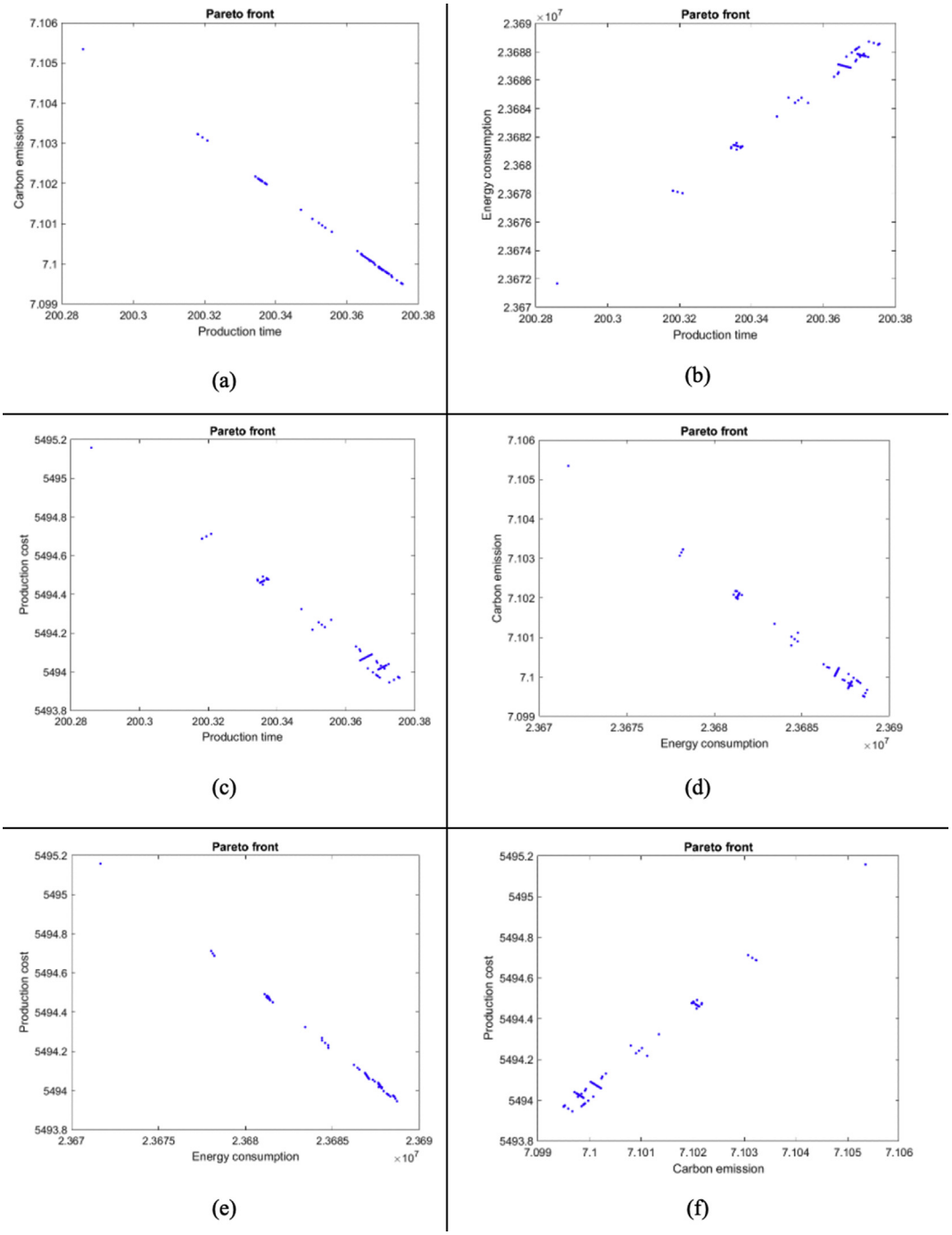

Figure 6. Pareto front of the objective functions for (a) carbon emission-production time, (b) energy consumption-production time, (c) production cost-production time, (d) carbon emission-energy consumption, (e) production time-energy consumption, and (f) production cost-carbon emission.

Table 9. Solution of multi-objective optimization.

Decision variable	Optimum solution	*U*	*SAI*
$N_{r,1} = 276.23$ rpm	$E_{total} = 3{,}143{,}778.23$ J	0.0946	0.9054
$N_{r,2} = 311.86$ rpm			
$N_{r,3} = 345.81$ rpm			
$f_{r,1} = 0.28$ mm/rev	$T_{total} = 729.14$ s		
$f_{r,2} = 0.28$ mm/rev			
$f_{r,3} = 0.25$ mm/rev			
$d_{r,1} = 2.50$ mm	$CE_{total} = 0.72$ kgCO_2		
$d_{r,2} = 2.50$ mm			
$d_{r,3} = 2.50$ mm			
$N_s = 469.59$ rpm	$PC_{total} =$ IDR 19,405.45		
$f_s = 0.10$ mm/rev			
$d_s = 2.50$ mm			

Table 10. Sets of experiments.

Control parameter	Value
$N_{r,1}$ (rpm)	[273.23, 274.23, 275.23, 276.23]
$N_{r,2}$ (rpm)	[308.86, 309.86, 310.86, 311.86]
$N_{r,3}$ (rpm)	[342.81, 343.81, 344.81, 345.81]
N_s (rpm)	[469.59, 470.59, 471.59, 472.59]
$f_{r,1}$ (mm/rev)	[0.25, 0.26, 0.27, 0.28]
$f_{r,2}$ (mm/rev)	[0.25, 0.26, 0.27, 0.28]
$f_{r,3}$ (mm/rev)	[0.22, 0.23, 0.24, 0.25]
f_s (mm/rev)	[0.10, 0.11, 0.12, 0.13]
$d_{r,1}$ (mm)	[2.50, 2.51, 2.52, 2.53]
$d_{r,2}$ (mm)	[2.50, 2.51, 2.52, 2.53]
$d_{r,3}$ (mm)	[2.50, 2.51, 2.52, 2.53]
d_s (mm)	[2.47, 2.48, 2.49, 2.50]

that the parameters $d_{r,1}$ and d_s can reduce the production time slightly. Although it decreases, high depth of cut generates a high temperature and load, which results in high energy consumption. This means that the electrical energy consumed will be increased and will harm the tool. Consequently, this results in high carbon emissions and production costs. Similar results of the sensitivity analysis can be observed in the sixth and seventh configurations.

Based on the analysis above, the cutting parameter setting has complex impacts on energy consumption, carbon emissions, production time, and production costs. Table 11 shows the effect of changes in the cutting parameters ($N_{r,1}, f_{r,1}, and\, d_{r,1}$) on the *SAI*. In general, the cutting parameters that increase the cutting force decrease *SAI*. Therefore, the manufacturing industry needs to pay attention to the changes in cutting parameters as they become the determinant of sustainable performance in the cutting process.

5. Conclusion and future work

This research developed an analytical optimization model for multi-pass turning operation in a CNC machine to minimize energy consumption, carbon emissions, production time, and production costs simultaneously. The energy consumption consists of cutting energy consumption and non-cutting energy consumption based on the black-box approach. The non-cutting energy consumption is included in the model because it has not been explored in previous research, especially the changes in spindle rotation. This research also considered some important constraints in the machining processes, such as the chip-tool interface temperature, tool life, and stable cutting region. Based on the results of the sensitivity analysis, the spindle rotation speed and feed rate in multi-pass turning are sensitive to the objective functions, whereas the depth of cut is not sensitive. This research can be extended to various directions. Further models could consider the tool wear conditions in a CNC turning to correspond to the real machining conditions. Further research can be directed toward the development of a metaheuristic method to efficiently find the optimal cutting parameters, such as multi-objective backtracking

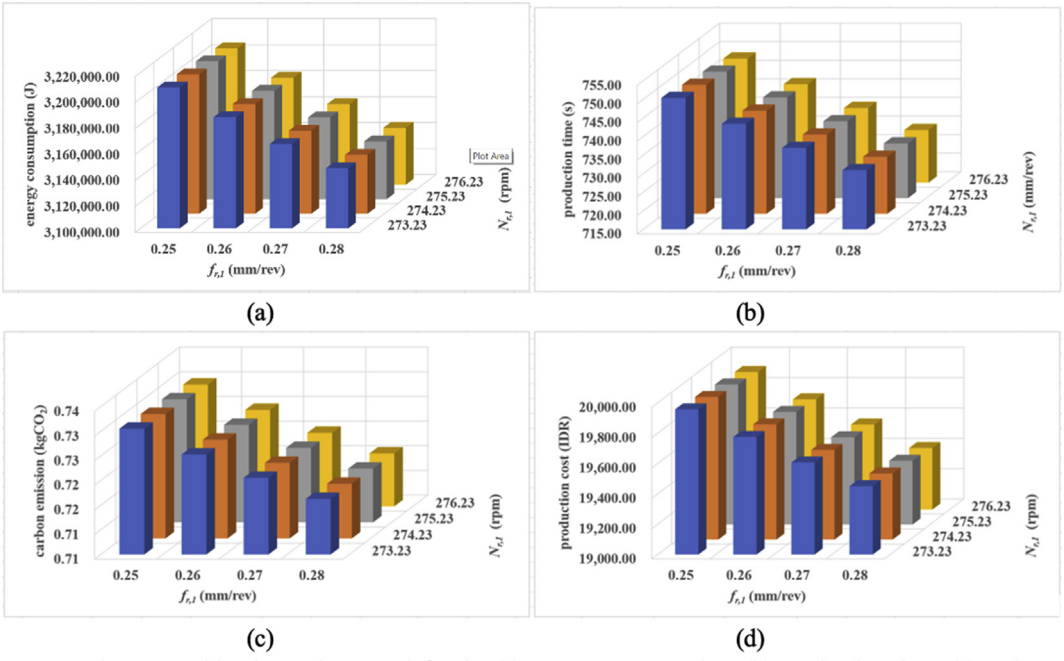

Figure 7. The 16 combinations of $N_{r,1}$ and $f_{r,1}$ for (a) energy consumption, (b) production time, (c) carbon emission and (d) production cost.

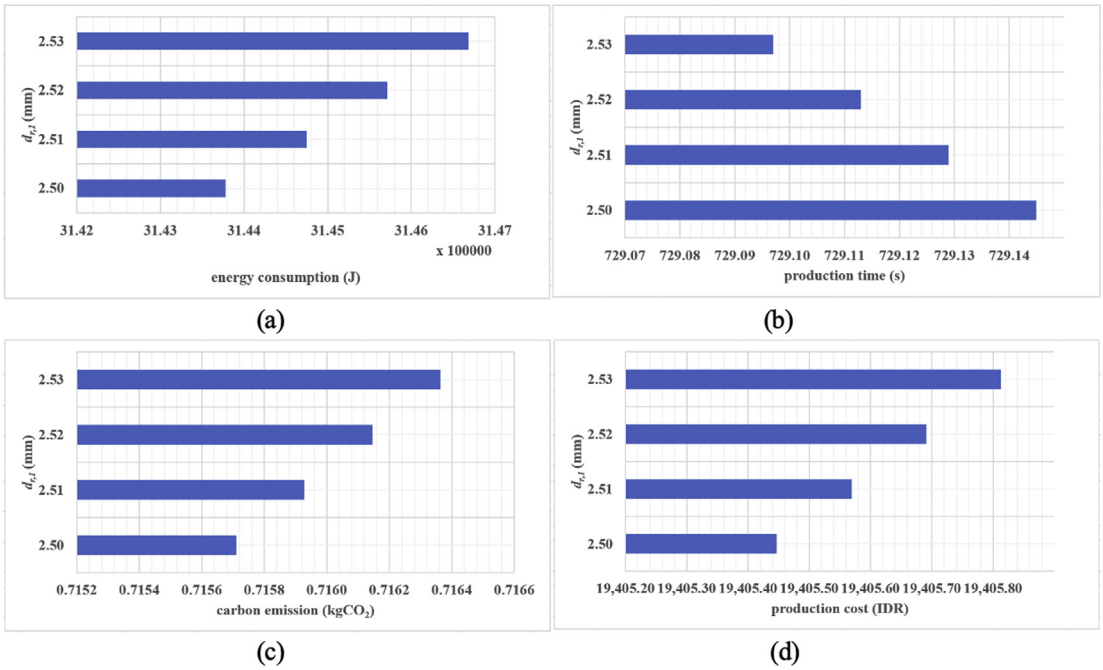

Figure 8. The 4 combinations of $d_{r,1}$ and d_s for (a) energy consumption, (b) production time, (c) carbon emission and (d) production cost.

Table 11. Sensitivity analysis of sustainability assessment index.

$N_{r,1}$	$f_{r,1}$	$d_{r,1}$	*SAI*
273.23	0.25	2.50	0.8823
274.23	0.25	2.50	0.8829
275.23	0.25	2.50	0.8836
276.23	0.25	2.50	0.8842
273.23	0.26	2.50	0.8900
274.23	0.26	2.50	0.8906
275.23	0.26	2.50	0.8913
.	.	.	.
.	.	.	.
274.23	0.28	2.50	0.9043
275.23	0.28	2.50	0.9048
276.23	**0.28**	**2.50**	**0.9054**
273.23	0.25	2.51	0.8822
274.23	0.25	2.51	0.8829
.	.	.	.
.	.	.	.
274.23	0.27	2.53	0.8975
275.23	0.27	2.53	0.8981
276.23	0.27	2.53	0.8987
273.23	0.28	2.53	0.9035
274.23	0.28	2.53	0.9040
275.23	0.28	2.53	0.9046
276.23	0.28	2.53	0.9051

search, decomposition-based archiving approach, and bare-bones multi-objective particle swarm optimization. In addition, the optimal results need to be verified with a real-machining experiment, which has not been conducted in this research because of time constraints and the need to develop some measuring devices.

Declarations

Author contribution statement

Phengky Pangestu: Conceived and designed the experiments; Performed the experiments; Wrote the paper.

Eko Pujiyanto: Analyzed and interpreted the data; Wrote the paper.

Cucuk Nur Rosyidi: Contributed reagents, materials, analysis tools or data; Wrote the paper.

Funding statement

This work was supported by Lembaga Penelitian dan Pengabdian Masyarakat Universitas Sebelas Maret (452/UN27.21/PN/2020).

Data availability statement

No data was used for the research described in the article.

Declaration of interests statement

The authors declare no conflict of interest.

Additional information

No additional information is available for this paper.

References

Amaranti, R., Irianto, D., Govindaraju, R., 2017. Green manufacturing: kajian literatur. In: Seminar Dan Konferensi Nasional IDEC 2017. Surakarta: Teknik Industri Universitas Sebelas Maret, pp. 171–181.

Ashbolt, S.C., Maheepala, S., Perera, B.J.C., 2017. Interpreting a Pareto set of operating options for water grids: a framework and case study. Hydrol. Sci. J. 62 (16), 2631–2654.

Awad, M., Khanna, R., 2015. Multiobjective optimization. In: Efficient Learning Machines. Apress, Berkeley, CA.

Bagaber, S.A., Yusoff, A.R., 2019. Energy and cost integration for multi-objective optimisation in a sustainable turning process. Measurement 136, 795–810.

Bringas, J.E., 2004. Handbook of Comparative World Steel Standards. ASTM International, West Conshohocken.
Camposeco-Negrete, C., 2015. Optimization of cutting parameters using response surface method for minimizing energy consumption and maximizing cutting quality in turning of AISI 6061 T6 aluminum. J. Clean. Prod. 91, 109–117.
Chauhan, P., Pant, M., Deep, K., 2015. Parameter optimization of multi-pass turning using chaotic PSO. Int. J. Machine Learning Cybernetics 6 (2), 319–337.
Chen, M.C., Tsai, D.M., 1996. A simulated annealing approach for optimization of multi-pass turning operations. Int. J. Prod. Res. 34 (10), 2803–2825.
Eaton, R.J., 1999. Getting the most out of environmental metrics. Bridge 29 (1), 4–7.
Garcia, S., Trinh, C.T., 2019. Comparisons of multi-objective evolutionary algorithms to solve the modular cell design problem for novel biocatalysis. Processes 7, 361.
Gaudencio, J.H.D., de Almeida, F.A., Turrioni, J.B., Quinino, R.C., Balestrassi, P.P., de Paiva, A.P., 2019. A multiobjective optimization model for machining quality in the AISI 12L14 steel turning using fuzzy multivariate mean square error. Precission Eng. 56, 303–320.
Groover, M.P., 2012. Fundamentals of Modern Manufacturing: Materials, Processes, and Systems, fifth ed. Wiley, Hoboken.
Gunantara, N., 2018. A review of multi-objective optimization: methods and its applications. Cogent Eng. 5 (1), 1502242.
Guo, Y., Duflou, J.R., Qian, J., Tang, H., Lauwers, B., 2015. An operation-mode based simulation approach to enhance the energy conservation of machine tools. J. Clean. Prod. 101, 348–359.
He, K., Tang, R., Jin, M., 2017. Pareto fronts of machining parameters for trade-off among energy consumption, cutting force and processing time. Int. J. Prod. Econ. 185, 113–127.
Henig, M.I., Buchanan, J.T., 1997. Tradeoff directions in multiobjective optimization problems. Math. Program. 78, 357–374.
Hu, L., Liu, Y., Lohse, N., Tang, R., Lv, J., Peng, C., Evans, S., 2017. Sequencing the features to minimise the non-cutting energy consumption in machining considering the change of spindle rotation speed. Energy 139, 935–946.
Hu, L., Liu, Y., Peng, C., Tang, W., Tang, R., Tiwari, A., 2018. Minimising the energy consumption of tool change and tool path of machining by sequencing the features. Energy 147, 390–402.
Hu, L., Tang, R., Cai, W., Feng, Y., Ma, X., 2019. Optimisation of cutting parameters for improving energy efficiency in machining process. Robot. Comput. Integrated Manuf. 59, 406–416.
International Energy Agency, 2007. Tracking Industrial Energy Efficiency and CO_2 Emissions. Stedia Media, Paris.
Jawahir, I.S., Dillon, O.W., 2007. Sustainable manufacturing processes: new challenges for developing predictive models and optimization techniques. In: Proceeding of the First International Conference on Sustainable Manufacturing. Aerospace Manufacturing Technology Centre, Montreal, pp. 1–19.
Jia, S., 2014. Energy Demand Modelling and Intelligent Computing of Machining Process for Low Carbon Manufacturing. Zhejiang University, Hangzhou.
Li, C., Tang, Y., Cui, L., Yi, Q., 2013. Quantitative analysis of carbon emissions of CNC-based machining systems. In: Proceedings of IEEE 10th International Conference on Networking, Sensing and Control. IEEE, Evry, pp. 869–874.
Liu, Z.J., Sun, D.P., Lin, C.X., Zhao, X.Q., Yang, Y., 2016. Multi-objective optimization of the operating conditions in a cutting process based on low carbon emission costs. J. Clean. Prod. 124, 266–275.
Lu, C., Gao, L., Lu, X., Chen, P., 2016. Energy-efficient multi-pass turning operation using multi-objective backtracking search algorithm. J. Clean. Prod. 137, 1516–1531.
Lv, J., Tang, R., Jia, S., 2014. Therblig-based energy supply modelling of computer numerical machine tools. J. Clean. Prod. 65, 168–177.
Marler, R.T., Arora, J.S., 2004. Survey of multi-objective optimization methods for engineering. Struct. Multidiscip. Optim. 26 (6), 369–395.
Marler, R.T., Arora, J.S., 2005. Function-transformation methods for multi-objective optimization. Eng. Optim. 37 (6), 551–570.
Mativenga, P.T., Rajemi, M.F., 2011. Calculation of optimum cutting parameters based on minimum energy footprint. CIRP Ann. - Manuf. Technol. 60, 149–152.
National Development & Reform Commission of China (NDRC), 2013. Baseline Emission Factors for Regional Power Grids in China. Retrieved from. http://www.ccchina.gov.cn/archiver/cdmcn/UpFile/Files/Default/20130917081426863466.pdf.
Onwubolu, G.C., Kumalo, T., 2001. Optimization of multipass turning operations with genetic algorithms. Int. J. Prod. Res. 39 (16), 3727–3745.
Rao, R.K., Rai, D.P., Balic, J., 2017. A new multiobjective algorithm for optimization of modern machining processes. Eng. Appl. Artif. Intell. 61, 103–125.
Rosyidi, C.N., Imamah, N.U.F., Jauhari, W.A., 2020. An optimization model of make or buy decision and quality improvement of components using rebate. Cogent Eng. 7 (1), 1767266.
Sada, S.O., 2020. The use of multi-objective algorithm (MOGA) in optimizing and predicting weld quality. Cogent Eng.
Shin, Y.C., Joo, Y.S., 1992. Optimization of machining conditions with practical constraints. Int. J. Prod. Res. 30 (12), 2907–2919.
Sihag, N., Sangwan, K.S., 2019. Development of a sustainability assessment index for machine tools. Procedia CIRP 80, 156–161.
Tian, C., Zhou, G., Zhang, J., Zhang, C., 2019. Optimization of cutiing parameters considering tool wear conditions in low-carbon manufacturing environment. J. Clean. Prod. 226, 706–719.
Vipin, Arora, B.B., Mishra, R.S., 2011. Optimization of machining time at multi-pass turning in heavy machining operation. Int. J. Eng. Stud. 3 (1), 13–20.
Widhiarso, W., Rosyidi, C.N., 2018. Multi objective optimization model for minimizing production cost and environmental impact in CNC turning process. In: The 3rd International Conference on Industrial, Mechanical, Electrical, and Chemical Engineering. Surakarta: AIP Conference Proceedings, 030024-1 - 030024-7.
Yi, Q., Li, C., Tang, Y., Chen, X., 2015. Multi-objective parameter optimization of CNC machining for low carbon manufacturing. J. Clean. Prod. 95, 256–264.
Yin, R., Ke, J., Mendis, G., Sutherland, J.W., 2019. A cutting parameter-based model for cost and carbon emission optimisation in a NC turning process. Int. J. Comput. Integrated Manuf. 32 (10), 919–935.
Zhong, Q., Tang, R., Peng, T., 2017. Decision rule for energy consumption mini mization during material removal process in turning. J. Clean. Prod. 140, 1819–1827.
Zhou, G., Zhou, C., Lu, Q., Tian, C., Xiao, Z., 2017. Feature-based carbon emission quantitation strategy for the part machining process. Int. J. Comput. Integrated Manuf. 31 (4-5), 406–425.